

# Analytical Model of Concrete-Filled Fiber-Reinforced Polymer Tubes based on Multiaxial Constitutive Laws

Chang-Geun Cho<sup>1</sup>; Minh Kwon, M.ASCE<sup>2</sup>; and Enrico Spacone, A.M.ASCE<sup>3</sup>

**Abstract:** A model is proposed for predicting the compression behavior of axially loaded concrete cylinders confined by fiber reinforced polymer (FRP) shells. To capture the active confinement applied by the FRP, an orthotropic hypoelasticity-based constitutive law is used for the concrete. This law is defined the triaxial stress space. The confinement-induced concrete strength enhancements are computed from a four-parameter failure surface. The corresponding peak strain increase is computed using a newly proposed strain enhancement factor. The FRP shell behavior is modeled using a stress-strain relation for plane stress orthotropic laminated composites. The proposed model is implemented into an incremental approach for the analysis of compression tests. No iterations are needed to find the stresses corresponding to prescribed axial strains. The model is verified with correlation studies with different experimental tests on concrete-filled FRP cylinders.

**DOI:** 10.1061/(ASCE)0733-9445(2005)131:9(1426)

**CE Database subject headings:** Concrete; Confinement; Fiber reinforced polymers; Constitutive relations; Compression tests; Tubes.

## Introduction

It is well established that the behavior of concrete in the loading direction is greatly influenced by the presence of confining stresses in the other principal directions. A large volume of research has been conducted to enhance the concrete response, particularly in terms of ductility, by introducing confinement provided, for example, by transverse reinforcement and tubes. In recent years, fiber-reinforced polymers (FRP) have been introduced as a new class of strengthening materials. While the traditional confinement by steel hoops or spirals provides constant confining stresses after steel yielding (passive confinement), the FRP jacket provides a linearly increasing confinement during the full loading range (active confinement) up to rupture of the FRP jacket. In this contest, Kwon and Spacone (2002) developed a three-dimensional (3D) concrete constitutive model that can reproduce the linearly increasing confinement provided by the FRP transverse reinforcement. Even though the above 3D model can trace the increase in strength and ductility with sufficient accuracy, its computational demand is too high. To describe the effects of confinement, Pantazopoulou and Mills (1995) proposed an explicit formula relating the concrete lateral strain to the axial strain.

This formula cannot however readily describe the continuously varying confinement provided by the FRP jacket. Samaan et al. (1998) proposed a simple closed-form confinement model based on the relation between the concrete dilation rate and the stiffness of the confining jacket. The above model, however, does not include failure criteria for the FRP jacket. Spoelstra and Monti (1999) developed an implicit approach to capture the confinement effects due to the FRP jacket. They extended the model by Mander et al. (1988), originally proposed for the constant confinement due to steel, to the varying confinement due to the FRP transverse reinforcement. This is however an implicit approach that requires iterations in the constitutive laws and its computational cost may be too high for the analysis of large-scale structures. Furthermore, since the FRP shells are modeled as isotropic materials, even though they are laminated composite shells, the ply properties do not contribute to the confinement effect. The enhancements in strength and strain are determined by fitting the confined concrete stress-strain curve to available test results.

Fam and Rizkalla (2001) proposed a variable-confinement concrete model for concrete-filled FRP tubes. This is an extension of the confinement model by Mander et al. (1988) and considers a biaxial strength failure criterion of the FRP tubes. Davol et al. (2001) proposed a model for the compressive behavior of the FRP-confined concrete that uses an equivalent tangent modulus that varies as a function of the lateral strain. The properties of the FRP shells are obtained from the classical lamination theory, which allows the shell ply properties to be considered in the confinement calculations. A limited number of experimental tests are used to calibrate the confinement model. The model by Davol et al. (2001) uses an iterative procedure to compute the current apparent Poisson's ratio. Becque et al. (2003) introduced a model for concrete-filled FRP tubes that uses a triaxial concrete law based on the octahedral theory by Gerstle (1981). In Gerstle's model, concrete is treated as an isotropic material, though concrete manifests stress-induced anisotropy. Gerstle's model traces the concrete nonlinear response through the evolution of the bulk and the deviatoric moduli. The bulk modulus is used to trace Poisson's effect, but the bulk modulus goes to infinity as Pois-

<sup>1</sup>Researcher, Research Institute for Disaster Prevention, E2-118, Kyungpook National Univ., Sankyuk-Dong 1370, Puk-Ku, Taegu, 702-170, Korea. E-mail: chocg70@hanmail.net

<sup>2</sup>Assistant Professor, Dept. of Civil Engineering and Engineering Research Institute, Gyeongsang National Univ., Jinju, Gyeongnam, 660-701, Korea (corresponding author). E-mail: kwonm@gsnu.ac.kr

<sup>3</sup>Professor, Dept. PRICOS, Faculty of Architecture, Univ. "G. D'Annunzio", Pescara, Italy. E-mail: espacone@unich.it

Note. Associate Editor: Dat Duthinh. Discussion open until February 1, 2006. Separate discussions must be submitted for individual papers. To extend the closing date by one month, a written request must be filed with the ASCE Managing Editor. The manuscript for this paper was submitted for review and possible publication on April 15, 2003; approved on February 10, 2005. This paper is part of the *Journal of Structural Engineering*, Vol. 131, No. 9, September 1, 2005. ©ASCE, ISSN 0733-9445/2005/9-1426-1433/\$25.00.

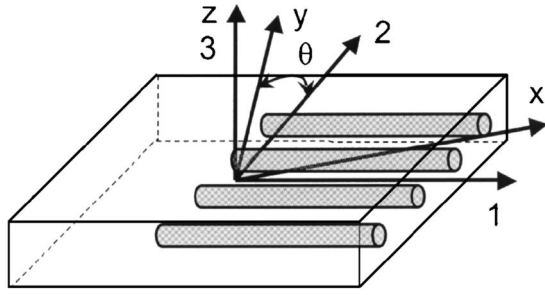


Fig. 1. Lamina in local and global coordinates

son's ratio approaches 0.5. This is clearly a problem, as several tests on both unconfined and FRP-confined concrete have shown apparent Poisson's ratios that increase well beyond 0.5 [Mirmiran and Shahawy (1997) observed, for example, values around 0.8].

The present paper proposes an explicit incremental model for predicting the compressive behavior of FRP-confined concrete. Concrete is treated as an orthotropic material described by a triaxial constitutive law based on a hypoelastic formulation. The directions of orthotropy are parallel to the principal stress directions. The confinement effects are determined from the current concrete triaxial stress state. The behavior of the FRP shells is modeled using a plane stress orthotropic laminated law for the composite material. The proposed model is verified via correlation studies with available experimental tests.

## Fiber-Reinforced Polymer Jacket Constitutive Law

### Lamina of Fiber-Reinforced Polymer Material

The FRP materials used in this study consist of strong fibers embedded in a relatively weak matrix. The jackets are assembled from individual plies. An individual lamina is composed of unidirectional fibers in a continuous matrix and each laminate contains fibers with different orientations in order to obtain the desired properties of the assembled laminate.

### Classical Lamination Theory

The classical lamination theory is used to describe the behavior of the laminated composite material. The assumptions of the classical lamination theory are clearly stated by Jones (1999). Since each individual lamina of the FRP laminated jacket is composed of unidirectional fibers embedded in a matrix, it can be modeled as a transversely isotropic material in the plane normal to the fiber direction, as shown in Fig. 1. The material coordinates (1,2,3) are introduced for a lamina. Direction 1 is parallel to the fiber direction, Direction 3 is normal to the lamina, and Direction 2 completes the coordinate system. The stress-strain relation for a lamina with respect to the material coordinates can be expressed as:

$$\begin{Bmatrix} \sigma_1 \\ \sigma_2 \\ \tau_{12} \end{Bmatrix} = \begin{bmatrix} Q_{11} & Q_{12} & 0 \\ Q_{21} & Q_{22} & 0 \\ 0 & 0 & Q_{33} \end{bmatrix} \begin{Bmatrix} \varepsilon_1 \\ \varepsilon_2 \\ \gamma_{12} \end{Bmatrix} \quad (1)$$

The coefficients of the constitutive matrix  $\mathbf{Q}$  in Eq. (1) are

$$Q_{11} = E_1 / (1 - \nu_{12}\nu_{21})$$

$$Q_{22} = E_2 / (1 - \nu_{12}\nu_{21})$$

$$Q_{12} = Q_{21} = E_2\nu_{12} / (1 - \nu_{12}\nu_{21})$$

$$Q_{33} = G_{12} \quad (2)$$

where  $E_1$ =modulus of the composite lamina in the fiber direction;  $E_2$ =modulus normal to the fiber direction in the plane of the lamina;  $\nu_{ij}$ =Poisson's ratio for the deformation in the  $j$  direction when the loading acts in the  $i$  direction; and  $G_{12}$ =in-plane shear modulus. To obtain the stress-strain relation in the structure coordinate system ( $x, y, z$ ), Eq. (1) must be rotated. The stress-strain relation in the structure coordinate system can be rewritten as

$$\boldsymbol{\sigma} = \bar{\mathbf{Q}}\boldsymbol{\varepsilon} \quad (3)$$

where  $\boldsymbol{\sigma} = \{\sigma_x, \sigma_y, \tau_{xy}\}^T$ =stress vector;  $\boldsymbol{\varepsilon} = \{\varepsilon_x, \varepsilon_y, \gamma_{xy}\}^T$ =strain vector; and the material matrix  $\bar{\mathbf{Q}}$  can be determined from  $\mathbf{Q}$  by coordinate transformation.

### Laminate Equivalent In-Plane Properties

The resultant forces and moments acting upon a laminate are determined by integrating the stresses in each layer or lamina through the thickness of the laminate. The equivalent orthotropic in-plane properties of a laminated composite can be derived from those of a symmetric laminate where there is no shear coupling. If the  $x$  and  $y$  directions in Fig. 1 are set to the longitudinal and the hoop direction of a cylinder, respectively, the relation between strain and resultant forces for a laminate shell in the structural coordinate system is expressed as follows

$$\begin{Bmatrix} \varepsilon_L \\ \varepsilon_H \\ \gamma_{LH} \end{Bmatrix} = \begin{bmatrix} \frac{1}{tE_L} & -\frac{\nu_{LH}}{tE_L} & 0 \\ -\frac{\nu_{LH}}{tE_L} & \frac{1}{tE_H} & 0 \\ 0 & 0 & \frac{1}{tG_{LH}} \end{bmatrix} \begin{Bmatrix} N_L \\ N_H \\ N_{LH} \end{Bmatrix} \quad (4)$$

where the equivalent orthotropic in-plane properties are:

$$E_L = \frac{A_{11}A_{22} - A_{12}^2}{tA_{22}}, \quad E_H = \frac{A_{11}A_{22} - A_{12}^2}{tA_{11}}$$

$$\nu_{LH} = \frac{A_{12}}{A_{22}}, \quad \nu_{HL} = \frac{A_{12}}{A_{11}}, \quad G_{LH} = \frac{A_{66}}{t} \quad (5)$$

$$A_{ij} = \sum_{k=1}^n (\bar{Q}_{ij})_k (h_k - h_{k-1})$$

where  $h_k$ =the distance from the midplane of the lamina to each ply; and subscripts  $L$  and  $H$  indicate longitudinal and hoop directions, respectively.  $E_L$  and  $E_H$ =elastic moduli in the longitudinal and hoop directions, respectively.  $\nu_{HL}$  and  $\nu_{LH}$ =Poisson's ratios.  $t$ =the laminate thickness.  $N_L$ =force resultant in the longitudinal direction;  $N_H$ =force resultant in the hoop direction; and  $N_{LH}$ =the shear force resultant.

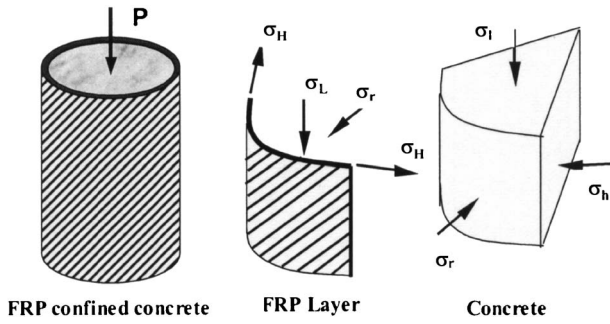


Fig. 2. Stresses in the fiber-reinforced polymer-confined concrete cylinder

### Fiber-Reinforced Polymer Jacket Failure Criteria

The Tsai-Wu or Tsai-Hill failure criterion is commonly used for orthotropic composites (Jones 1999). The failure criteria of the orthotropic composite materials are typically written in the structure coordinate system. In the present model, however, the failure of the FRP tube is written in the material coordinate system of the local fibers. Since the axial stress developed in the FRP tube is relatively small compared to that of the concrete, the degradation of the tensile stresses due to the stresses in the axial direction is neglected. With these assumptions, it is assumed that the tube has failed when one of its plies has exceeded its strength in the fiber direction. To determine the ply stresses, it is necessary to first transform the strains in the structure coordinate system into strains in the local ply coordinate system. The ply stresses are then computed based on the ply constitutive law. Once the stresses in the material coordinate system are known, they are compared to the fiber strength. This criterion is also used in the model proposed by Davol et al. (2001).

### Incremental Model for Concrete-Filled Fiber-Reinforced Polymer Jackets

As shown in Fig. 2, it is assumed that the shell is thin when compared to the radius of the section and that the strain gradient in the shell is negligible. Thus, for a circular section, the bending stiffness of the laminate has no effect on the section analyses and the equivalent in-plane properties can be used.

#### System Stress-Strain Relations

The shell is assumed to be in a biaxial stress state with stresses acting along the longitudinal ( $\sigma_L$ ) and lateral directions ( $\sigma_H$ ), which become principal directions. The shear terms ( $N_{LH}$ ) in Eq. (4) becomes zero. The longitudinal and hoop strain of the FRP shell is therefore determined as

$$\begin{aligned} \varepsilon_L &= \frac{\sigma_L}{E_L} - \nu_{HL} \frac{\sigma_H}{E_H} \\ \varepsilon_H &= \frac{\sigma_H}{E_H} - \nu_{LH} \frac{\sigma_L}{E_L} \end{aligned} \quad (6)$$

As for the concrete response, the triaxial stress state influences the concrete strength and its ductile behavior. Changes in the confining stresses due to the FRP jacket affect the concrete re-

sponse. The concrete triaxial strain-stress relation is based on an orthotropic hypoelastic formulation and is expressed through the following incremental law

$$\begin{Bmatrix} d\varepsilon_l \\ d\varepsilon_r \\ d\varepsilon_h \end{Bmatrix} = \begin{bmatrix} 1/E_l & -\mu_{lr}/\sqrt{E_l E_r} & -\mu_{lh}/\sqrt{E_l E_h} \\ & 1/E_r & -\mu_{rh}/\sqrt{E_r E_h} \\ \text{sym.} & & 1/E_h \end{bmatrix} \begin{Bmatrix} d\sigma_l \\ d\sigma_r \\ d\sigma_h \end{Bmatrix} \quad (7)$$

where  $E_l$ ,  $E_r$ , and  $E_h$ =concrete tangent moduli in the axial, radial, and hoop directions, respectively; and  $\mu_{ij}$ =derived from Poisson's ratios  $\nu_{ij}$  as:

$$\mu_{lr}^2 = \nu_{lr}\nu_{rl}, \quad \mu_{rh}^2 = \nu_{rh}\nu_{hr}, \quad \mu_{lh}^2 = \nu_{lh}\nu_{hl} \quad (8)$$

If the concrete properties in the radial and hoop directions are assumed to be identical, then

$$\sigma_r = \sigma_h, \quad \varepsilon_r = \varepsilon_h, \quad E_r = E_h, \quad \mu_{lr} = \mu_{rh} \quad (9)$$

and Eq. (7) becomes:

$$\begin{Bmatrix} d\varepsilon_l \\ d\varepsilon_r \end{Bmatrix} = \begin{bmatrix} 1/E_l & -2\mu_{lr}/\sqrt{E_l E_r} \\ -\mu_{lr}/\sqrt{E_l E_r} & (1 - \mu_{rh})/E_r \end{bmatrix} \begin{Bmatrix} d\sigma_l \\ d\sigma_r \end{Bmatrix} \quad (10)$$

The strain-stress relation in Eq. (10) can be inverted to obtain the stress-strain relation:

$$\begin{Bmatrix} d\sigma_l \\ d\sigma_r \end{Bmatrix} = \frac{1}{\Omega} \begin{bmatrix} E_l(1 - \mu_{rh}^2) & 2\mu_{lr}\sqrt{E_l E_r}(1 + \mu_{rh}) \\ \mu_{lr}\sqrt{E_l E_r}(1 + \mu_{rh}) & E_r(1 - \mu_{rh}) \end{bmatrix} \begin{Bmatrix} d\varepsilon_l \\ d\varepsilon_r \end{Bmatrix} \quad (11)$$

where  $\Omega = 1 - 2\mu_{lr}^2(1 + \mu_{rh}) - \mu_{rh}^2$ .

The equivalent uniaxial strain concept introduced by Darwin and Pecknold (1977) is used here to convert the two-dimensional coupled constitutive relations of Eq. (11) into two independent uniaxial constitutive relations. The incremental concrete axial stress is written as

$$d\sigma_l = E_l d\varepsilon_{ul} \quad (12)$$

where  $\varepsilon_{ul}$ =concrete equivalent uniaxial strain defined as follows

$$\varepsilon_{ul} = [(1 - \mu_{rh}^2)\varepsilon_l + 2\mu_{lr}\sqrt{E_l E_r}(1 + \mu_{rh})\varepsilon_r]/\Omega \quad (13)$$

From the assumption of perfect bond and thus no slip between the concrete and the FRP tube, compatibility and equilibrium in the cross section shown in Fig. 3 are expressed as follows:

$$\begin{aligned} \varepsilon_L &= \varepsilon_l, \quad \varepsilon_H = \varepsilon_r \\ \sigma_H &= -\frac{\sigma_r R}{t} \end{aligned} \quad (14)$$

where  $R$ =radius of the concrete core; and  $t$ =total thickness of the FRP shell. Combining Eqs. (6) and (14), the concrete incremental

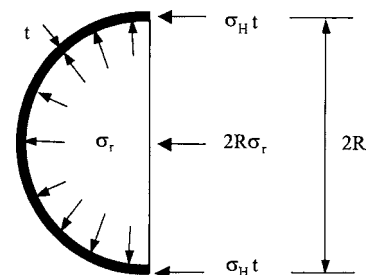


Fig. 3. Section equilibrium in the hoop direction

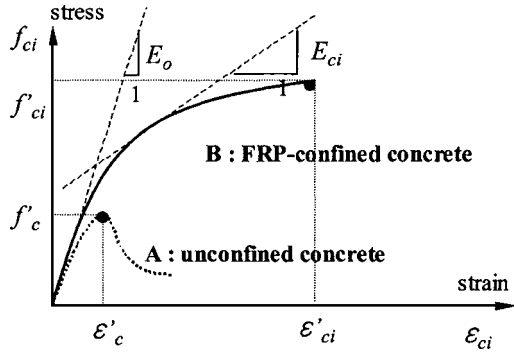


Fig. 4. Compressive stress-strain relations of fiber-reinforced polymer-confined concrete

radial stress  $d\sigma_r$  and the FRP shell incremental axial stress  $d\sigma_L$  are written in the following forms:

$$d\sigma_r = -\frac{(v_{LH}d\varepsilon_l + d\varepsilon_r)E_H t}{(1 - v_{HL}v_{LH})R} \quad (15)$$

$$d\sigma_L = E_L \left( d\varepsilon_L - d\sigma_r \frac{v_{HL}R}{v_H t} \right) \quad (16)$$

The incremental concrete radial strain is derived from Eqs. (10) and (16):

$$d\varepsilon_r = d\varepsilon_l \left[ \frac{v_{LH}E_H t(1 - \mu_{rh} - 2\mu_{lr}^2) + \mu_{lr}\sqrt{E_t E_r R}(1 - v_{HL}v_{LH})}{-E_r R(1 - v_{HL}v_{LH}) - E_H t(1 - \mu_{rh} - 2\mu_{lr}^2)} \right] \quad (17)$$

### Confined Concrete Triaxial Constitutive Law

In Fig. 4, the uniaxial compressive behavior of unconfined concrete is denoted as A and the compressive behavior of concrete confined by the FRP shell is denoted as B. The curve proposed by Saenz (1964) is used as the uniaxial stress-strain curve of unconfined concrete.

As the concrete confinement increases, the concrete response changes from brittle to rather ductile. At the same time, the concrete compressive strength becomes considerably higher than the unconfined uniaxial compressive strength. In order to reasonably describe the confinement effects on the concrete response, a triaxial compressive model should be used. In this study, to predict the increased compressive strength due to confinement in the  $\sigma_r$ ,  $\sigma_h$ ,  $\sigma_l$  stress space, the ultimate strength surface of the confined concrete is expressed by the four-parameter failure surface proposed by Hsieh et al. (1979):

$$f(I_1, J_2, \sigma_r) = a\bar{J}_2 + b\sqrt{\bar{J}_2} + c\bar{\sigma}_r + d\bar{I}_1 - 1 = 0 \quad (18)$$

where

$$\bar{\sigma}_r = \frac{\sigma_r}{f'_c}$$

$$\bar{I}_1 = \frac{\sigma_r + \sigma_h + \sigma_l}{f'_c}$$

$$\bar{J}_2 = \frac{(\sigma_r - \sigma_h)^2 + (\sigma_h - \sigma_l)^2 + (\sigma_l - \sigma_r)^2}{6(f'_c)^2} \quad (19)$$

The values of the four parameters,  $a=2.018$ ,  $b=0.9714$ ,  $c=9.1421$ , and  $d=0.2312$ , were determined based on the available uniaxial and biaxial tests by Kupfer et al. (1969) and on the triaxial tests of Mills and Zimmerman (1970).

The assumption  $\sigma_r = \sigma_h$  is made, thus Eq. (18) can be simplified. The increased concrete compressive strength is expressed in the form

$$f'_{ci} = \lambda_{si} f'_c \quad (20)$$

where  $f'_c$ =concrete uniaxial unconfined compressive strength; and  $\lambda_{si}$ =strength enhancement factor, defined as the ratio of confined to unconfined concrete strength.  $\lambda_{si}$  can be determined from the failure surface of concrete. With the above notation Eq. (18) can be written in the following form:

$$f(\gamma\bar{\sigma}_r, \gamma\bar{\sigma}_h, \gamma\bar{\sigma}_l) = 0 \quad (21)$$

where  $\bar{\sigma}_h = \sigma_h/f'_c$ ,  $\bar{\sigma}_l = \sigma_l/f'_c$ ,  $\gamma$ =multiplier; and  $\gamma\bar{\sigma}_r, \gamma\bar{\sigma}_h, \gamma\bar{\sigma}_l$ =multiples of the normalized stress and define the distance from the origin to the failure surface along the  $\bar{\sigma}_r, \bar{\sigma}_h, \bar{\sigma}_l$  directions. Solution of Eq. (21) leads to a quadratic equation of the form

$$\gamma^2 + p\gamma - q = 0 \quad (22)$$

where

$$p = \frac{b\sqrt{\bar{J}_2} + c\bar{\sigma}_r + d\bar{I}_1}{a\bar{J}_2}$$

$$q = \frac{1}{a\bar{J}_2}$$

By solving the roots of the above quadratic equation,  $\gamma$  is computed and the strength enhancement factor  $\lambda_{si}$  is calculated from  $\gamma\bar{\sigma}_r, \gamma\bar{\sigma}_h, \gamma\bar{\sigma}_l$ , respectively.

Experiments have also shown that confined concrete shows a response that is more ductile than that of unconfined concrete. Though a strain failure surface is required to predict the maximum compressive strain, a strain failure surface is difficult to formulate from available experimental data. To account for the increased ductility of confined concrete, Selby (1993) proposed a strain enhancement factor,  $\lambda_{ei}$ , for concrete triaxial stress states. The model proposed by Selby (1993) was based on the experimental results of Kupfer et al. (1969) and Rechart et al. (1928). However, this confinement model was proposed for passive

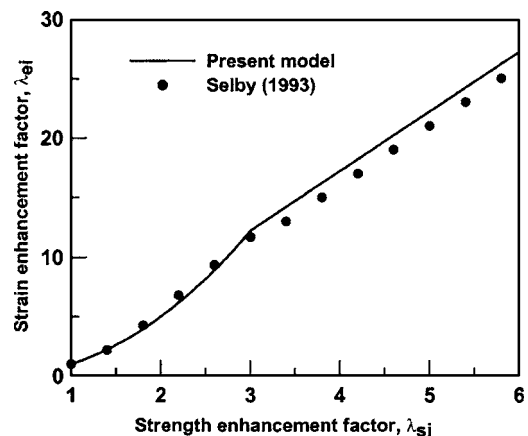


Fig. 5. Strain enhancement factor versus strength enhancement factor

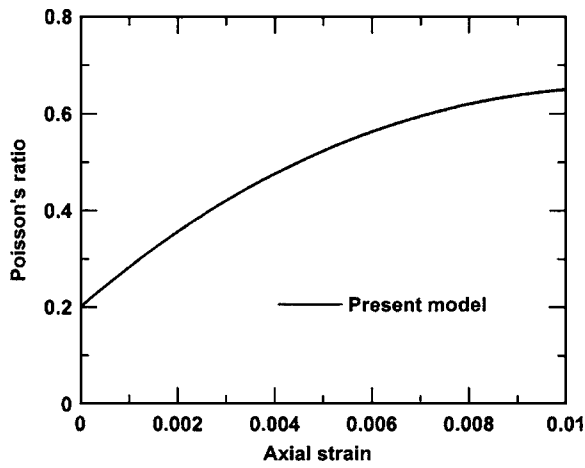


Fig. 6. Variation of concrete Poisson's ratio as a function of the axial strain

(steel) confinement, and needs to be revised for active (FRP) confinement. The following expressions for the strain enhancement factors are proposed in this study:

$$\begin{aligned} \text{if } \lambda_{si} \leq 3 \quad \lambda_{ei} &= 0.6 + 0.4(4\lambda_{si}^2 - 2\lambda_{si} - 1) \\ \text{if } \lambda_{si} > 3 \quad \lambda_{ei} &= 5\lambda_{si} - 2.8 \end{aligned} \quad (23)$$

The comparison between the expressions in Eq. (23) and those proposed by Selby (1993) is shown in Fig. 5. Hence, the maximum compressive strain of the confined concrete  $\epsilon'_{ci}$  is expressed as

$$\epsilon'_{ci} = \lambda_{ei} \epsilon'_c \quad (24)$$

where  $\epsilon'_c$  = maximum uniaxial compressive strain of the unconfined concrete. Following the above equations, the longitudinal tangent modulus of the concrete confined by the FRP shell,  $E_c$ , can be computed from the concrete stress-strain curve with the peak stresses and strains computed according to Eqs. (20) and (24), respectively.

Previous studies on FRP-confined concrete by Mirmiran and Shahawy (1997) and Davol et al. (2001) assume that the concrete radial tangent modulus is equivalent to the longitudinal tangent modulus. Such an assumption is not generally true but the radial modulus is very difficult to measure during experiments. The present study uses the experimental results by Mirmiran and Shahawy (1997), Picher et al. (1996), and Kawashima et al. (1997) to define an expression of the concrete radial modulus that depends linearly on the strength enhancement factor and on the concrete longitudinal modulus:

$$E_r = \lambda_{si}^{0.4} E_l \quad (25)$$

A significant volumetric expansion is observed during experiments on concrete subjected to high compressive strains. Based on the expression proposed by Elwi and Murray (1979), which was obtained from the experimental results by Kupfer and Gerstle (1973), the following cubic equation is adopted for Poisson's ratio  $\nu_{ci}$  in the  $i$ th direction as a function of the corresponding compressive uniaxial strain  $\epsilon_{ci}$

$$\nu_{ci} = \nu_o \left[ 1 + \alpha \frac{\epsilon_{ci}}{\epsilon'_c} + \beta \left( \frac{\epsilon_{ci}}{\epsilon'_c} \right)^2 + \gamma \left( \frac{\epsilon_{ci}}{\epsilon'_c} \right)^3 \right] \quad (26)$$

where  $\alpha = 1.763$ ,  $\beta = -5.36$ , and  $\gamma = 8.586$ . The relation between axial compressive strain and Poisson's ratio is shown in Fig. 6.

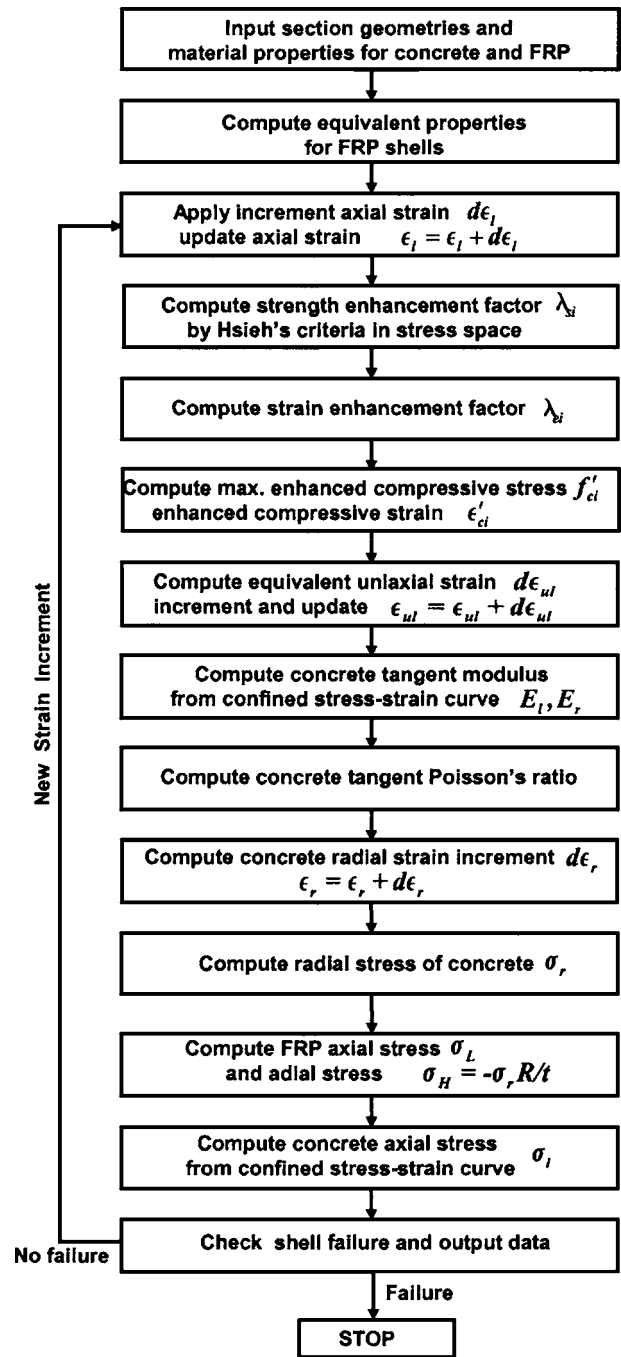
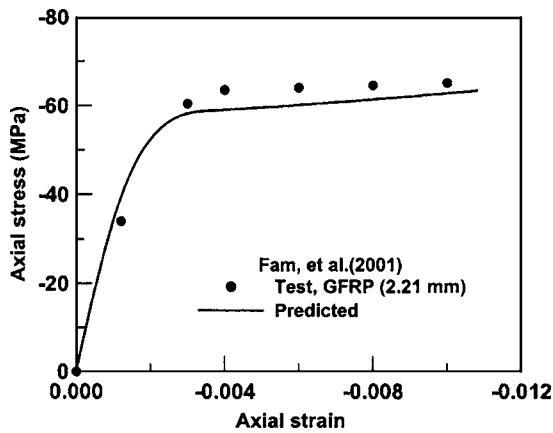


Fig. 7. Flow chart of model for fiber-reinforced polymer-confined concrete cylinders

### Nonlinear Algorithm for the Incremental Analysis of Concrete-Filled Fiber-Reinforced Polymer Tubes

The incremental analysis procedure for concrete-filled FRP tubes under pure compression is summarized in the flow chart of Fig. 7. For each compression strain increment, the FRP shell is checked for failure of the FRP tube. The analysis stops upon reaching failure of the FRP shell. The proposed model accounts for, on the one hand, the confinement effect of the FRP shell, and on the other the triaxial behavior of the concrete. The FRP shell effects depend on the number of shell layers, the direction of each layer, the layer stiffness, and the layer thickness. The triaxial concrete



**Fig. 8.** Glass fiber-reinforced polymer-confined concrete cylinders by Fam and Rizkalla (2001): experimental and numerical results

response is accounted for through the 3D constitutive law discussed above, which is based on an orthotropic hypoelasticity formulation.

### Numerical Examples and Verification

In order to validate the proposed model, a set of correlation studies between available experimental tests and numerical results are presented. The correlation studies refer to five experimental investigations on axially loaded concrete-filled FRP cylinders.

Fam and Rizkalla (2001) performed uniaxial compression tests on concrete filled-glass FRP (GFRP) cylinders. The cylinders had a 219 mm diameter and were 438 mm high. The total thickness of the GFRP shell with nine layers was 2.21 mm. The fibers were placed with angles of  $-88^\circ/-88^\circ/+4^\circ/-88^\circ/-88^\circ/+4^\circ/-88^\circ/+4^\circ/-88^\circ$  with respect to the longitudinal direction. The longitudinal and hoop elastic moduli of the GFRP shell were 19.8 GPa and 33.4 GPa, respectively. The longitudinal and hoop strength of the GFRP shell was 183 MPa and 548 MPa, respectively. The GFRP shell Poisson's ratio was 0.055. The uniaxial unconfined strength of the concrete was  $f'_c = 58$  MPa. The unconfined concrete compressive strain corresponding to  $f'_c$  was 0.002. Fig. 8 compares the axial stress-axial strain responses of the numerical results and of the experimental results. The numerical results

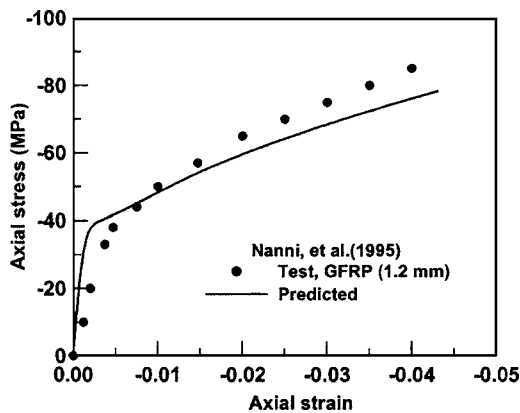


**Fig. 9.** Glass fiber-reinforced polymer-confined concrete cylinders by Nanni and Bradford (1995): experimental and numerical results

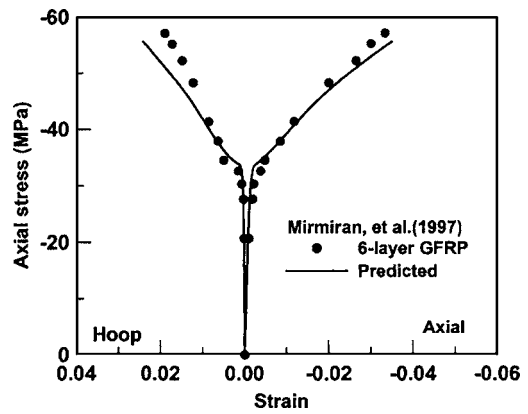


**Fig. 10.** Glass fiber-reinforced polymer-confined concrete cylinders by Mirmiran and Shahawy (1997): experimental and numerical results

show a lower strength prediction, but overall the numerical results correlate well with the experiment tests along the entire loading history.

The model predictions were also compared with the experimental test by Nanni and Bradford (1995). The test was performed on a concrete-filled GFRP tube having a 152.5 mm diameter and a 305 mm height. The concrete uniaxial strength was 36.3 MPa and the total thickness of the GFRP tube (made of four layers) was 1.2 mm. All fibers were placed at a  $90^\circ$  angle with respect to the longitudinal direction of the specimen. The elastic modulus and strength of the GFRP shell were 52 MPa and 583 MPa, respectively. Fig. 9 shows the comparison of the axial stress-axial strain relations of the GFRP-confined concrete between the numerical and the experimental results. The predicted behavior closely follows the measured result. However, as with the case shown in Fig. 8, the numerical results predict a higher stiffness at the early loading stage. This is probably due to the assumption of perfect bond between the FRP shell and the concrete.

In order to validate the strain responses of the proposed model in the lateral as well as in the longitudinal direction, the tests conducted by Mirmiran and Shahawy (2001) were analyzed. The experiments were performed using GFRP cylinders with a 152.5 mm diameter and a 305 mm height. The fibers were placed with angles of  $\pm 15^\circ$  with respect to the longitudinal direction. Two

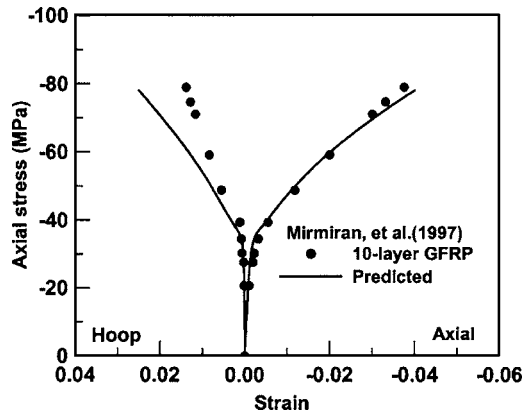


**Fig. 11.** Glass fiber-reinforced polymer-confined concrete by Mirmiran and Shahawy (1997): experimental and numerical results

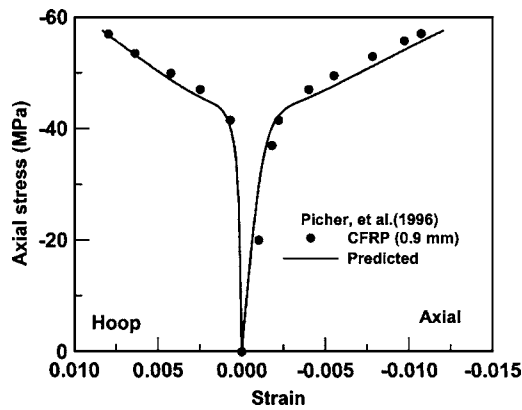


Fig. 12. Carbon fiber-reinforced polymer-confined concrete by Picher et al. (1996): experimental and numerical results

specimens were studied. The specimens were wrapped with six and ten plies, and the resulting total thickness of the FRP shell was 1.3 mm and 2.1 mm, respectively. The elastic modulus of each fiber was 40.74 GPa and the strength was 641 MPa. The unconfined concrete uniaxial strength was 32 MPa. Figs. 10 and 11 show the comparison between the numerical and the experimental results for the six-layer-FRP shell and for the ten-layer-FRP shell, respectively. The predicted responses in the longitudinal stress and strain are close to the experimental responses, though the hoop strains are slightly overestimated. The thicker shell shows significant increases in peak stress and ultimate strain capacity.

Picher et al. (1996) performed uniaxial compression tests on concrete cylinders wrapped by carbon FRP (CFRP). The cylinder had a 152 mm diameter and a 304 mm height. The CFRP consisted of three layers of carbon fibers and the total thickness of the CFRP shell was 0.9 mm. The fibers were placed with a 90° angle with respect to the longitudinal direction. The elastic modulus of the carbon fiber was 83 GPa and its strength was 1245 MPa. The uniaxial compressive strength of the unconfined concrete is 39.7 MPa. The axial and lateral responses of the numerical and of the experimental results are compared in Fig. 12. The predicted results on stiffness and ultimate strength agree well with the experimental results both in the longitudinal and in the lateral directions.

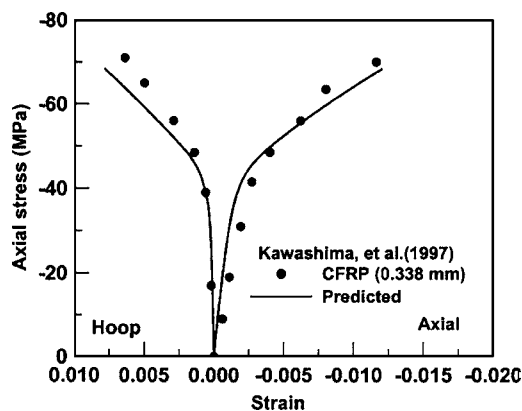


Fig. 13. Carbon fiber-reinforced polymer-confined concrete by Kawashima et al. (1997): experimental and numerical results

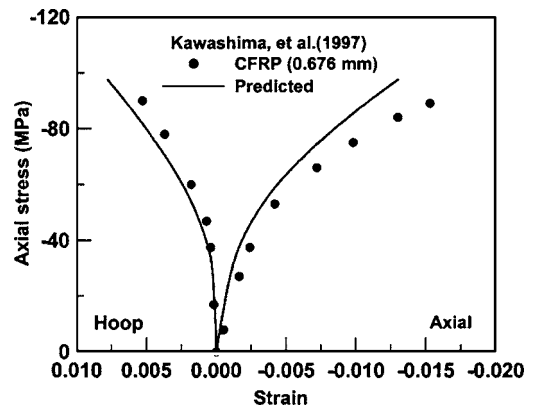


Fig. 14. Carbon fiber-reinforced polymer-confined concrete by Kawashima et al. (1997): experimental and numerical results

Finally, the experimental results of tests performed by Kawashima et al. (1997) were compared with the numerical results obtained with the proposed model. The experiments were performed on reinforced concrete specimens confined with CFRP tubes. The core concrete was reinforced with a 1% steel ratio and the CFRP shells were 0.338 mm and 0.676 mm thick. The longitudinal steel is modeled as elastic perfectly plastic with a perfect bond to the concrete. The fiber tensile strengths in the two different specimens were 2,810 MPa (for the thinner shell) and 2,327 MPa (for the thicker shell). The elastic modulus of the fibers was 439 GPa and the concrete uniaxial compressive strength was 39 MPa. Fig. 13 shows the numerical and the experimental results of the specimen wrapped with the 0.338 mm thick CFRP shell and Fig. 14 refers to the specimen wrapped with the 0.676 mm thick CFRP shell. In the earlier loading stage, the predicted behaviors of both the axial and the hoop strains are close to the experimental results. The numerical predictions have a small discrepancy around the peak strength, but overall the analytical results show a good correlation with the experimental results. The specimen wrapped with the thicker shell showed significant increases in ultimate compressive stress and strain capacities.

## Conclusions

This study presents an incremental model for the analysis of axially loaded concrete-filled FRP shells. To capture the active confinement effects due to the FRP shell, the stress-strain behavior of the confined concrete is described by a constitutive law whose parameters are defined in a triaxial stress space. The confined concrete strength and its corresponding peak strain are computed from the triaxial failure surface. In order to accurately model the behavior and the failure of the FRP shells, a plane stress orthotropic model is used for the laminated composite material. The proposed model for the FRP-confined concrete cylinder is verified using correlation studies with data available from experimental tests. The proposed model adequately captures the behavior of compression tests with good estimates of the responses in terms of axial and radial strains and stresses. The main advantage of the proposed model is derived from its simplicity and accuracy. The model does not require any iterations to compute the concrete response corresponding to a given strain history. The model rationally predicts the compressive behavior of the confined concrete throughout the loading history for given FRP shell properties.

## Notation

The following symbols are used in this paper:

- $a, b, c, d$  = four parameters used in concrete failure surface;  
 $E_1, E_2$  = composite lamina moduli parallel and normal to the fiber direction;  
 $E_L, E_H$  = equivalent elastic moduli of fiber-reinforced polymer shell in the longitudinal and hoop directions;  
 $E_\ell, E_r, E_h$  = concrete tangent moduli in the longitudinal, radial, and hoop directions;  
 $f'_{ci}$  = concrete unconfined uniaxial compressive strength;  
 $G_{12}$  = in-plane lamina shear modulus;  
 $h_k$  = distance from the midplane of the lamina to each ply;  
 $N_L, N_H$  = the resultant force in longitudinal direction and hoop direction;  
 $N_{LH}$  = the resultant shear force;  
 $\mathbf{Q}, \mathbf{Q}$  = material matrices of the lamina in-plane stress-strain relation in the material and structure coordinates;  
 $R$  = concrete core radius;  
 $t$  = fiber-reinforced polymer shell total thickness;  
 $\gamma$  = normalizing factor for stress vector on failure surface;  
 $\epsilon$  = lamina strain vector in global coordinates;  
 $\epsilon_L, \epsilon_H, \gamma_{LH}$  = fiber-reinforced polymer shell longitudinal, hoop and shear strain, respectively;  
 $\epsilon_l, d\epsilon_l$  = concrete total and incremental strains in longitudinal direction;  
 $\epsilon_r, d\epsilon_r$  = concrete total and incremental strains in and strain increment in radial direction;  
 $\epsilon_{ul}, d\epsilon_{ul}$  = concrete total and incremental equivalent uniaxial strain;  
 $\epsilon'_{ci}$  = concrete strain corresponding to  $f'_{ci}$ ;  
 $\lambda_{si}, \lambda_{ei}$  = strength and strain enhancement factors;  
 $\nu_{12}, \nu_{21}$  = lamina Poisson's ratios;  
 $\nu_{LH}, \nu_{HL}$  = fiber-reinforced polymer shell equivalent Poisson's ratios;  
 $\nu_{ci}$  = concrete Poisson's ratio;  
 $\nu_o$  = concrete initial Poisson's ratio;  
 $\sigma$  = lamina stress vector in global coordinates;  
 $\sigma_L, d\sigma_L$  = fiber-reinforced polymer shell total and incremental stresses in longitudinal direction;  
 $\sigma_H, d\sigma_H$  = fiber-reinforced polymer shell total and incremental stresses in hoop direction;  
 $\sigma_l, d\sigma_l$  = concrete total and incremental stresses in longitudinal direction;  
 $\sigma_r, d\sigma_r$  = concrete total and incremental stresses in radial direction; and  
 $\Omega$  = denominator in concrete constitutive matrix.

## References

Becque, J., Patnaik, A. K., and Rizkalla, S. H. (2003). "Analytical models for concrete confined with FRP tubes." *J. Compos. Constr.*, 7(1),

- 31–38.  
 Darwin, D., and Pecknold, D. A. (1977). "Nonlinear biaxial stress-strain law for concrete." *J. Eng. Mech. Div.*, 103(2), 229–241.  
 Davol, A., Burgueño, R., and Seible, F. (2001). "Flexural behavior of circular concrete filled FRP shells." *J. Struct. Eng.*, 127(7), 810–817.  
 Elwi, A. A., and Murray, D. W. (1979). "A 3D hypoelastic concrete constitutive relationship." *J. Eng. Mech. Div.*, 105(4), 623–641.  
 Fam, A. Z., and Rizkalla, S. H. (2001). "Confinement model for axially loaded concrete confined by circular fiber-reinforced polymer tubes." *ACI Struct. J.*, 98(4), 451–461.  
 Gerstle, K. H. (1981). "Simple formulation of biaxial concrete behavior." *ACI J.*, 78(1), 62–68.  
 Hsieh, S. S., Chen, W. F., and Ting, E. C. (1979). "An elastic-fracture model for concrete." *ASCE Proc. 3d Eng. Mech. Div. Spec. Conf.*, ASCE, Reston, Va., 437–440.  
 Jones, M. J. (1999). "Mechanics of composite materials." 2nd Ed., Taylor & Francis.  
 Kawashima, K., Hosotani, M., and Hoshikuma, J. (1997). "A model for confinement effect for concrete cylinders confined by carbon fiber sheets." *NCEER-NICEDE Workshop on Earthquake Engineering Frontiers in Transportation Facilities*, NCEER, State Univ. of New York, Buffalo, N.Y.  
 Kupfer, H. B., and Gerstle, K. H. (1973). "Behavior of concrete under biaxial stresses." *J. Eng. Mech. Div.*, 99(4), 852–866.  
 Kupfer, H. B., Hildorf, H. K., and Rusch, H. (1969). "Behavior of concrete under biaxial stresses." *ACI J.*, 66(8), 656–666.  
 Kwon, M., and Spacone, E. (2002). "Three-dimensional finite element analyses of reinforced concrete columns." *Comput. Struct.*, 80(8), 199–212.  
 Mander, J. B., Priestley, M. J., and Park, R. (1988). "Theoretical stress-strain model for confined concrete." *J. Struct. Eng.* 114(8), 1804–1826.  
 Mills, L. L., and Zimmerman, R. M. (1970). "Compressive strength of plain concrete under multiaxial loading conditions." *ACI J.*, 67(10), 802–807.  
 Mirmiran, A., and Shahawy, M. (1997). "Behavior of concrete columns confined by fiber composites." *J. Struct. Eng.*, 123(5), 583–590.  
 Nanni, A., and Bradford, N. M. (1995). "FRP jacketed concrete under uniaxial compression." *Constr. Build. Mater.*, 9(2), 115–124.  
 Pantazopoulou, S. J., and Mills, R. H. (1995). "Microstructural aspects of the mechanical response of plain concrete." *ACI Mater. J.*, 92, 605–616.  
 Picher, F., Rochette, P., and Labossiere, P. (1996). "Confinement of concrete cylinders with CFRP." *Proc., 1st Int. Conf. on Composites in Infrastructure*, H. Saadatmanesh and M. R. Ehsani, eds., Univ. of Arizona, Tucson, Ariz., 829–841.  
 Rechart, F. E., Brandzaeg, A., and Brown, R. L. (1928). "A study of the failure of concrete under combined compressive stresses." Bull. No. 185, Univ. of Illinois Engineering Experimental Station, Urbana, Ill.  
 Saenz, L. P. (1964). "Discussion of equation for the stress-strain curve of concrete by Desayi and Krishman." *ACI J.*, 61(9), 1229–1235.  
 Samaan, M., Mirmiran, A., and Shahawy, M. (1998). "Model of concrete confined by fiber composites." *J. Struct. Eng.*, 124(9), 1025–1031.  
 Selby, R. G. (1993). "Three-dimensional constitutive relations for reinforced concrete." PhD thesis, Univ. of Toronto, Toronto.  
 Spoelstra, M. R., and Monti, G. (1999). "FRP-confined concrete model." *J. Compos. Constr.*, 3(3), 143–150.